CrossMark

Horizontal and vertical distributions of ^{137}Cs in seabed sediments around the river mouth near Fukushima Daiichi Nuclear Power Plant

Tadahiko Tsuruta[1] · Hisaya Harada[2] · Toshiharu Misonou[1] · Toshiyuki Matsuoka[1] ·
Yasuyuki Hodotsuka[3]

Abstract Investigations including a bathymetric survey, sonic prospecting, and vibrocoring were performed to understand the horizontal and vertical distribution of ^{137}Cs in seabed sediments in shallow seas with depths less than 30 m near the Fukushima Daiichi Nuclear Power Plant. Especially, features of ^{137}Cs distributions in deeper sections of the seabed sediments were studied to evaluate the vertical heterogeneity of ^{137}Cs distribution in the seabed sediments in shallow seas. The distribution area of the seabed sediments was less than half of the investigation area, and the locations of the seabed sediments were divided into flat and terrace-like seafloors based on their topographical features. The thicknesses of the seabed sediment layers were mostly <2 m. The ^{137}Cs inventories in the seabed sediments varied from 13 ± 1 to $3{,}510 \pm 26$ kBq m^{-2}, and continuous distributions of ^{137}Cs at depths greater than 81 cm were observed. The ^{137}Cs distributions were not uniform; however, the ^{137}Cs inventories tended to be larger near the base of the steeper ascending slopes than in the terrace-like seafloors themselves. Based on the relationship between the ^{137}Cs inventories and mean shear stress, features of the seafloor topography were inferred to be significant control factors governing the horizontal and vertical distribution of ^{137}Cs in the seabed sediments. Rapid changes and multiple peaks in the vertical profile of the ^{137}Cs distributions suggest that they are related to pulse input caused by heavy-rain events. Change in the ^{137}Cs inventories with depth in this study are larger than those reported in previous studies, indicating earlier results of ^{137}Cs inventories per unit in seabed sediments in shallow seas, especially near the river mouth, which drains a radiologically highly-contaminated basin, were underestimated.

1 Introduction

The Fukushima Daiichi Nuclear Power Plant (FDNPP) accident, which occurred following the Great East Japan Earthquake and the resulting tsunami in March 2011, resulted in extensive release of radioactive cesium into the Pacific Ocean, especially, ^{137}Cs with a half-life of 30.2 years. Understanding the features of ^{137}Cs transport from contaminated mountain forests to coastal sinks is key to the revitalization of marine industries. Therefore, evaluations of forest ecosystems and fluvial and lacustrine environments have been conducted (e.g., Funaki et al. 2014; Yamaguchi et al. 2014; Kitamura et al. 2014; Kurikami et al. 2014; Yamada et al. 2015; Dohi et al. 2015; Niizato et al. 2016).

^{137}Cs distribution in shallow seas, which are major settlement areas for particle-sorbed ^{137}Cs, is a very important factor when studying ^{137}Cs transport from contaminated mountain forests to coastal sinks. Several evaluations of the distribution of ^{137}Cs in seabed sediments have been conducted, and many are ongoing. For example, Ambe et al. (2014) reported high ^{137}Cs concentrations in the area south of the FDNPP at depths shallower than 100 m.

✉ Tadahiko Tsuruta
tsuruta.tadahiko@jaea.go.jp

1   Fukushima Environmental Safety Center, Japan Atomic Energy Agency, 10-2, Fukasaku, Miharu-machi, Fukushima 963-7700, Japan

2   SUNCHO Consultants CO., Ltd, 1-8-9, Kamedo, Koutou, Tokyo 136-0071, Japan

3   Ocean High Technology Institute, Inc., 2-29-12, Honmachi, Nakano, Tokyo 164-0012, Japan

Otosaka and Kato (2014) showed that more than 80% of the ^{137}Cs has accumulated in regions shallower than 100 m, which was likely attributed to the absorption of ^{137}Cs from radiologically contaminated seawater onto seabed sediments (Misumi et al. 2014). However, these studies have focused primarily on the dynamics of ^{137}Cs in oceanic seas with depths greater than 100 m (e.g., Otosaka and Kobayashi 2012; Kusakabe et al. 2013; Black and Buesseler 2014; Ono et al. 2015), and information about the distribution of ^{137}Cs in shallow seas is relatively limited. The numbers of data locations of ^{137}Cs distribution in seabed sediments in regions shallower than 50 m, as described in Kusakabe et al. (2013), Otosaka and Kato (2014), and Black and Buesseler (2014), are 4, 3, and 4, respectively. Moreover, these sampling locations were situated in river mouths that had highly contaminated river basins (e.g., Ukedo River Basin; Kitamura et al. 2014; Kurikami et al. 2014; Yamada et al. 2015). Insufficient data from, and sampling locations in, shallower regions are thought to have led to a poor understanding of the features of ^{137}Cs transport from contaminated mountain forests to coastal sinks. Data on ^{137}Cs concentrations in seabed sediments obtained by Tokyo Electric Power Co., Inc. (TEPCO 2016) make evaluating the movement of ^{137}Cs in shallow seas difficult owing to a lack of vertical ^{137}Cs profiles in seabed sediments. Thornton et al. (2013) and NRA (2016) used a towed gamma ray spectrometer along with a depth sensor and a bathymetric survey, which indicated a relationship between the ^{137}Cs concentrations in seabed sediments and the features of seafloor topography. However,

their results were insufficient to understand the vertical distribution of ^{137}Cs in seabed sediments in shallow seas.

In this study, we examine the heterogeneity of ^{137}Cs distribution in seabed sediments at sea depths <30 m. A bathymetric survey and sonic prospecting were conducted to map the occurrences of seabed sediments, and core sampling was performed to describe the vertical profile of ^{137}Cs distribution in seabed sediments. Based on these investigations, control factors for the horizontal and vertical distribution of ^{137}Cs in seabed sediments in a shallow sea were evaluated. Vertical ^{137}Cs profiles in seabed sediments obtained in previous studies have been insufficient to evaluate ^{137}Cs concentrations because information about the distribution of ^{137}Cs at the lowermost depths of seabed sediments was lacking owing to short core sampler lengths (most less than 20 cm). Therefore, we employed a longer core sampler, with a maximum length of approximately 100 cm, and fabricated vibrocoring methods.

2 Materials and methods

2.1 Investigation area

Investigations were conducted near the mouth of the Ukedo River, located approximately 5–10 km from the FDNPP (Fig. 1). Because the upper part of the Ukedo River Basin has high levels of radiological contamination, several studies and analyses have been conducted in this basin to examine the features of ^{137}Cs transport from

Fig. 1 Contamination map around Fukushima Daiichi Nuclear Power Plant and investigation area. The contamination map was drawn using the Environment Monitoring Database for the Distribution of Radioactive Substances released by the TEPCO Fukushima Daiichi NOO Accident© 2013 Nuclear Regulation Authority
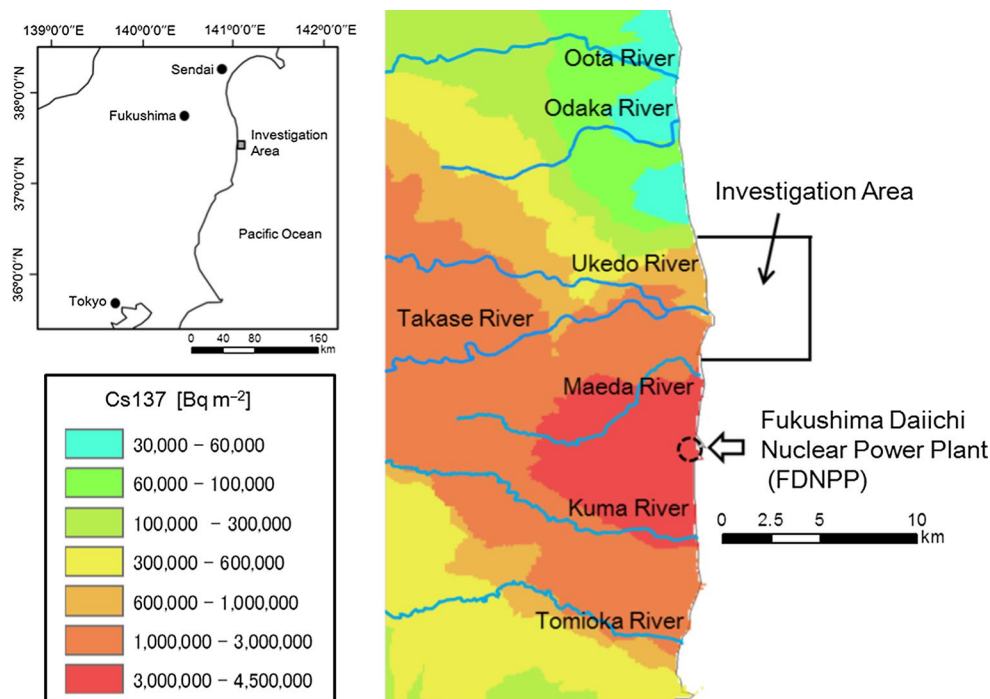
upstream to downstream (e.g., Kitamura et al. 2014; Kurikami et al. 2014; Yamada et al. 2015). The annual ^{137}Cs discharge from the Ukedo River into the Pacific Ocean in the first few years after the FDNPP accident was approximately 2.0 TBq, the highest among rivers in the region (Oota River: 0.27vTBq, Odaka River: 0.13 TBq, Maeda River: 0.4 TBq, Kuma River: 0.28 TBq, and Tomioka River: 0.11 TBq) (Kitamura et al. 2014).

Our sampling was performed approximately 5 km offshore at a depth of approximately 30 m, which was determined based on the results of models pertaining to the transport of Cs-contaminated sediments discharged from the river (Kitamura et al. 2015). A preliminary analysis conducted using the Regional Ocean Modeling System (ROMS) suggested that the primary settlement distance of fine-grained particles (0.02 mm; corresponding to silt based on the Wentworth grain-size scale) is <5 km from the river mouth (M. Itakura, unpublished personal communication, April 2013).

2.2 Investigation methods

### 2.2.1 Bathymetric survey and sonic prospecting

A bathymetric survey and sonic prospecting were conducted to map and interpret the characteristics of the seabed sediments from September to November 2013. For the bathymetric survey, PDR1300 W (Senbon Denki; depth range of up to 2 m) and Sonic 2024 (RS SONIC; sectors deeper than 2 m) echo sounders were used. The data were processed using MarineDiscovery4, and a bathymetric map with a resolution of 2–3 m was produced (Fig. 2).

Sonic prospecting involved a full-coverage side-scan sonar survey and a sub-bottom profile survey. The sonic prospecting data from the side-scan sonar were acquired using System3000 (L-3 Klein; depth range of up to 3 m) and 2000-DSS (Edge-Tech; sectors deeper than 3 m), and they were processed using the LampyrideEye4 software. As a result, side-scan sonar mosaics with a 0.5-m resolution (Fig. 3a) were obtained. The backscatter intensity value of these mosaics can be used to semi-qualitatively identify

Fig. 2 Bathymetric map and sampling points for vibrocoring
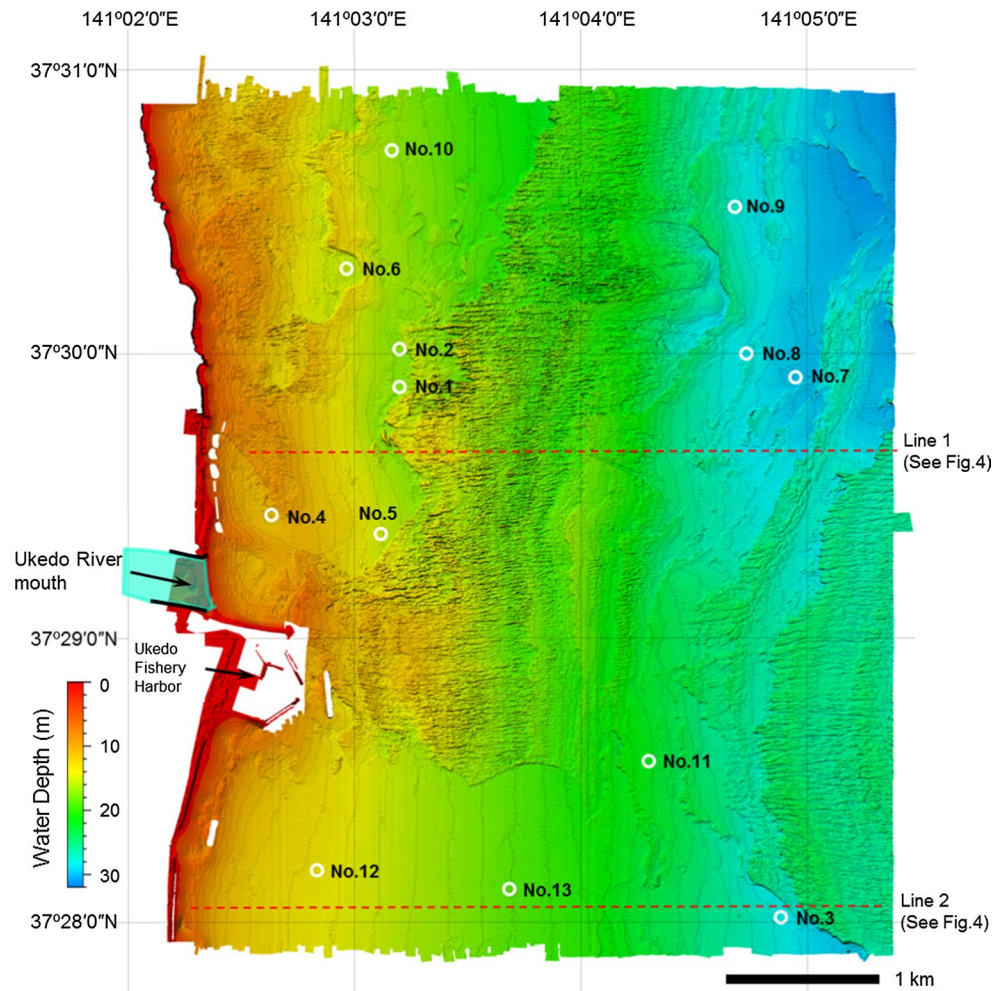
Fig. 3 **a** Sonar mosaics and **b** predicted seabed sediments map
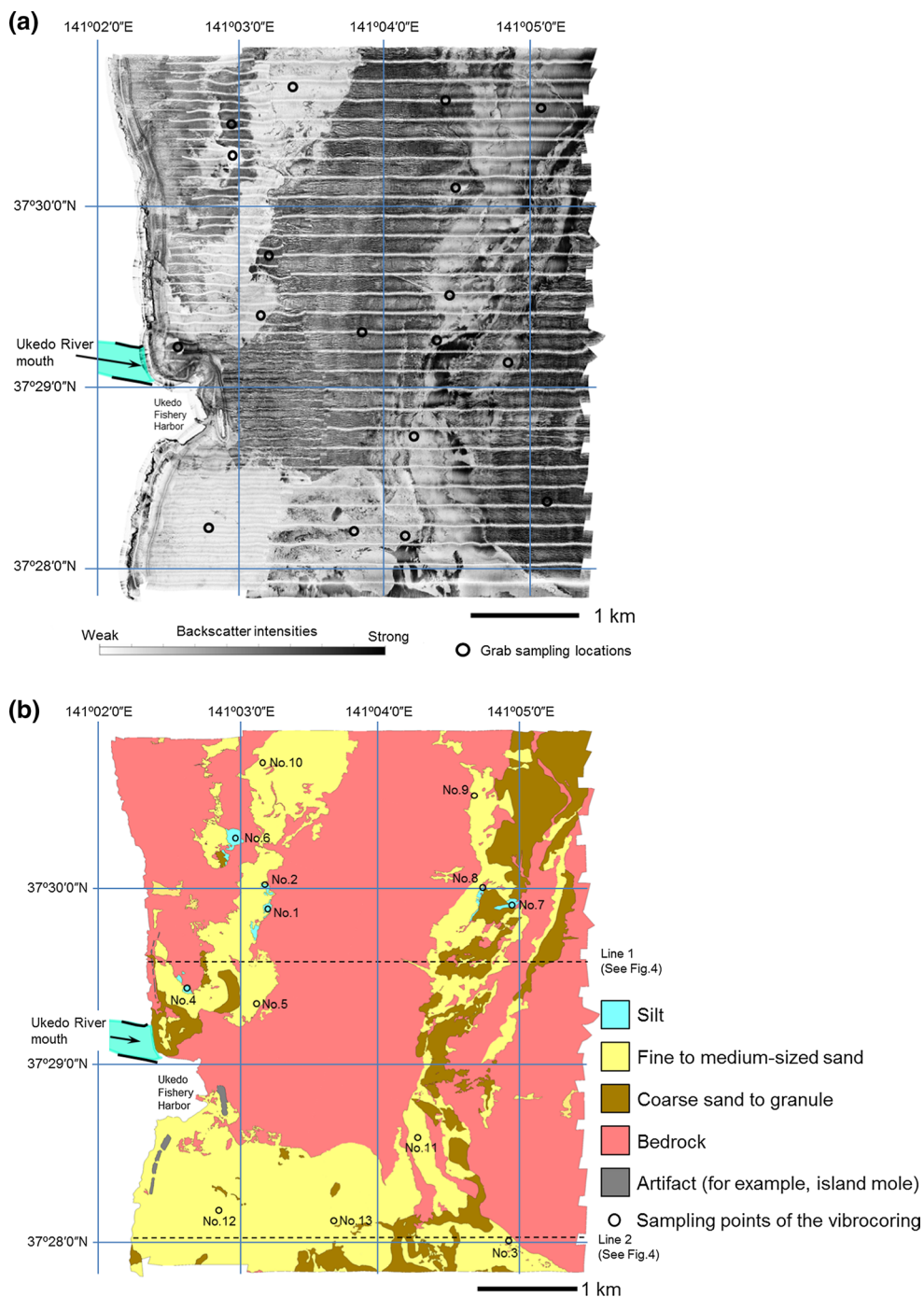
the type of seafloor (e.g., bedrock or sediments). Seabed sediment sampling was performed at 18 locations (Fig. 3a) by using a grab sampler (Smith–McIntyre); sediment types [clay, silt, sand (fine, medium, and coarse), and granule] were confirmed via visual observation. After comparing the backscatter intensity values with the results of seabed sediment sampling, the seafloor types in the investigation area were predicted (Fig. 3b). The areas with high backscatter intensities correspond to bedrock. The remaining areas, which were considered to be the distribution areas of seabed

sediments, were classified into three grain-size regions based on the features of backscatter intensity: coarse sand to granule, fine to medium sand, and silt. The major factors used for this classification are as follows: coarse sand to granule—high and spotted backscatter intensity; fine to medium sand—medium to low and pervasive backscatter intensity; and silt—very low and pervasive backscatter intensity.

Data about the sub-bottom profile were collected using BATHY2010 (SyQuest) in a depth range up to 3 m using 2000-DSS (Edge-Tech) in sectors deeper than 3 m. These

data were processed using the Seaprofile4 software package. The thickness of the seabed sediment overlying the bedrock was estimated based on an interpretation of the boundary between the seabed sediment and bedrock (Fig. 4).

2.2.2 Core sampling

Core sampling points were selected based on the results of the bathymetric survey and sonic prospecting, with a focus on the characteristic features of the seafloor topography. Vibrocoring, in which a core tube is driven into the seabed sediments by using the force of gravity enhanced by vibrational energy, was employed to collect deep seabed sediments. Seabed sediment core samples (tens of cm in length) were collected using polycarbonate tubes (diameter: 100 mm). In this study, the maximum and the average core lengths of the vibrocores were 81 cm and 45 cm, respectively. The seabed sediment cores sampled at depths of up to 50 cm and those sampled at depths greater than 50 cm were cut into 1 and 2-cm segments, respectively. The outer parts of the seabed sediment cores were excluded from the gamma-ray measurements to avoid vertical contamination. The obtained core sections were dried at 105 °C for approximately 1 d. Then, specific gamma rays of ^{134}Cs (605 keV and 796 keV) and ^{137}Cs (662 keV) were measured for 3600 s by using a high-purity germanium detector (GMX40P4-76, ORTEC® USA) with a detection limit of approximately 10 Bq kg^{-1}. From the measured results, the concentration and inventory of ^{137}Cs were calculated in units of Bq kg^{-1}

dry and Bq m^{-2}, respectively. The obtained values were corrected for decay based on the sampling date.

A grain-size analysis was conducted to evaluate the relationship between the concentration of ^{137}Cs and the grain size of the particles, using a procedure based on Japanese Industrial Standards (2009, JIS A 1204). The median grain size (D50 value) was determined from the cumulative grain size curve.

3 Results

3.1 Occurrence of seabed sediments

The bathymetric map shown in Fig. 2 and the water depth profiles shown in Fig. 4 indicate that the water depths at offshore distances of 1 km, 3 km, and 5 km were approximately 10 m (1/100 slope gradient), 20 m (1/150), and 30 m (1/166), respectively. Terrace-like seafloors consisting of steeper ascending slopes on their coastal sides (up-dip side) and gently descending slopes opposite to the coastal sides (dip side) (Fig. 4; Line 1) extend north of the Ukedo Fishery Harbor. The heights of the steeper ascending slopes are a few meters, and the lengths of gently descending slopes are about 1 km. This type of seafloor is probably a former shoreline, especially one equivalent to crest-type platforms (Mii 1962). A semicircular depression (diameter: 200 m; depth: 3 m) was observed on the seafloor starting about 3 km north of the Ukedo Fishery Harbor (around sampling point No. 6; Fig. 2). Flat seafloors (Fig. 4; Line 2) were observed south

Fig. 4 Water depth along *Lines 1* and *2*. The *solid line* shows the surface of the seafloor, and *green range* represents the distribution of seabed sediments
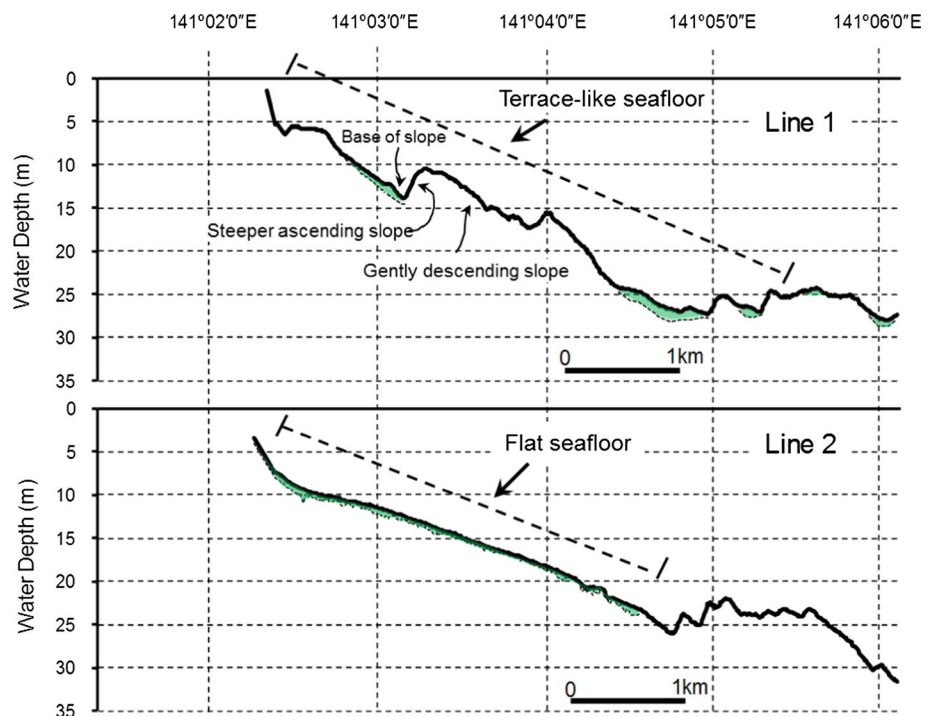
of the Ukedo Fishery Harbor. A gently inclined seafloor with a smooth plane was found to extend to about 3 km offshore.

As shown in Fig. 3b, bedrock, primarily comprising alternating beds of sandstone and siltstone (Pliocene Sendai Group, Mogi and Iwabuchi 1961; Kubo et al. 1994) is distributed in the investigation area. The occurrence of seabed sediments is restricted to the south of the Ukedo Fishery Harbor and in two elongated zones that are several hundreds of meters wide. Seabed sediments tend to accumulate at the base of the steeper ascending slopes in the elongated zones (Fig. 4; Line 1). To the south of the Ukedo Fishery Harbor, seabed sediments cover the flat seafloor homogeneously (Fig. 4; Line 2). The thicknesses of the seabed sediment layers are mostly less than 2 m, and the variation in layer thickness is small (Fig. 4). The surface ratio of bedrocks and seabed sediments is 65–35% (the total investigation area was about 30 km^2). Fine to medium sand (surface ratio of 24%) is the main constituent of the seabed sediments and coarse sand to granule-sized material (surface ratio of 10%) occurs relatively far from the shoreline. Silt is distributed in a quite narrow zone (surface ratio of 0.40%).

3.2 Spatial distribution of ^{137}Cs in seabed sediments

Table 1 summarizes locations, water depths, core lengths, and ^{137}Cs inventories of the vibrocoring samples. The sampling points and vertical changes in the ^{137}Cs activities (Bq m^{-2} cm^{-1}) and median grain size (D50 value) are shown in Figs. 4 and 5, respectively. The sampling points were selected based on the seafloor features: six core samplings (Nos. 1–6) were performed at the base of the steeper ascending slope (Fig. 4; Line 1), five core samplings (Nos. 7–11) on the gently descending slope toward offshore (Fig. 4; Line 2), and two core samplings (Nos. 12 and 13) on the flat seafloor (Table 1). Sampling point No. 6 was located at some distance from the steeper ascending slope. However, this point was located in a semicircular depression with steep sides, suggesting that the depositional features of seabed sediment at this point are strongly affected by the steeper ascending slope. Therefore, sampling point No. 6 was classified as the base of the steeper ascending slope.

The lengths of the vibrocores, approximately tens of cm (maximum length: 81 cm, average length: 45 cm), were longer than those used in previous studies, where multiple corers and triple-tube core samplers with average core lengths less than 20 cm were employed (Otosaka and Kato 2014; Ambe et al. 2014; Black and Buesseler 2014). However, despite using vibrocoring, seven cores (Nos. 1, 2, 4, 5, 8, 9, and 13) failed to capture the full extent of the ^{137}Cs inventory owing to insufficient core length. Therefore, the ^{137}Cs inventories of these cores were underestimated.

The ^{137}Cs inventories of the six sampling points (Nos. 1–6) ranged from 57 to 3510 kBq m^{-2} (Fig. 5). In general,

the ^{137}Cs inventory values collected at the base of the steeper ascending slope were greater than those at the other two locations (gently descending slope and flat seafloor; Table 1). In particular, the total ^{137}Cs inventory at point No. 6 (approximately 3500 kBq m^{-2}) was greater than the deposition value estimated using a towed gamma ray spectrometer near the mouth of the Ukedo River (approximately 20 kBq m^{-2}; NRA 2016), and greater than the average deposition value of the Ukedo River Catchment (2500 kBq m^{-2}; Yoshimura et al. 2015). Sampling point No. 6 was located in a semicircular depression with steep sides (Fig. 2). The degree of change in ^{137}Cs activity per cm of vertical depth (kBq m^{-2} cm^{-1}) was not uniform; ^{137}Cs activity decreased toward lower depths (Nos. 1, 2, and 3), increased toward lower depths (No. 4), and was almost the same at all depths from the surface to the bottom (No. 5). Sample No. 6 exhibited widely variable ^{137}Cs activity peaks and remarkably large peaks at depths of approximately 30 and 60 cm. The lowermost depths at which ^{137}Cs activities were found at sampling points Nos. 3 and 6 were approximately 29 and 72 cm, respectively. The ^{137}Cs activity of sampling point No. 5 extended to depths >81 cm. The grain sizes (D50 values) were homogeneous silt (Nos. 4 and 6), very fine–fine sand (Nos. 2, 3, and 5), and fine sand–coarse sand (No. 1).

The ^{137}Cs inventories of the five sampling points (Nos. 7–11) on the gently descending slope ranged from 13 to 175 kBq m^{-2} (Table 1); the degrees of change in the ^{137}Cs activities per cm of vertical depth (kBq m^{-2} cm^{-1}) were small, except at sampling point No. 9. The lowermost depths at which ^{137}Cs activities were found were 20–40 cm from the surface. The grain sizes (D50 values) were homogeneously fine sand (Nos. 9, 10, and 11), silt–fine (No. 8), and coarse sand (No. 7).

The ^{137}Cs inventories of the two sampling points (Nos. 12 and 13) located on the flat seafloor were 95 and 72 kBq m^{-2}, respectively. The degrees of change in the ^{137}Cs activities per cm of vertical depth (kBq m^{-2} cm^{-1}) increased with increasing depth. The grain sizes (D50 values) were homogeneous fine sand (No. 12) and silt–coarse sand (No. 13).

## 3.3 Relationship between ^{137}Cs concentration and grain size

The relationship between ^{137}Cs concentration (kBq kg^{-1}) and grain size showed general agreement with the findings of a previous report (Ambe et al. 2014), in which finer fractions tended to have higher ^{137}Cs concentrations (Fig. 6). The present study, in particular, revealed the ^{137}Cs concentrations of fractions finer (silt; <0.063 mm) than those reported in a previous paper (Ambe et al. 2014). However, at sampling points Nos. 5, 6, and 9, even though the grain size was almost constant, the ^{137}Cs concentrations varied by more than two orders of magnitude.

Table 1 Overview of vibrocoring results

Core no.	Sample name	Sampling date	North latitude	East longitude	Water depth (m)	Core length (cm)	Lowermost depth of ^{137}Cs[a] (cm)	^{137}Cs inventory Full extent of core	^{137}Cs inventory Upper 10 cm of core	Dominant grain size class[b]	Location
1	UKEE-140130-1	2014/1/30	37°29'53"N	141°3'12"E	14.4	54	N.D.	504 ± 9	96 ± 2	Silt–very fine sand	Base of steeper ascending slope
2	UKEE-140130-2	2014/1/30	37°30'1"N	141°3'12"E	14.3	44	N.D.	264 ± 6	56 ± 1	Very fine sand	Base of steeper ascending slope
3	UKEE-140227-5	2014/2/27	37°28'1"N	141°4'53"E	26.6	37	28	57 ± 9	29 ± 6	Very fine—fine sand	Base of steeper ascending slope
4	UKEE-140207-06	2014/2/7	37°29'26"N	141°2'38"E	7.9	29	N.D.	260 ± 5	72 ± 2	Silt	Base of steeper ascending slope
5	UKEE-140207-07	2014/2/7	37°29'22"N	141°37"E	12.0	81	N.D.	145 ± 6	21 ± 1	Fine sand	Base of steeper ascending slope
6	UKEE-140122-04	2014/1/22	37°30'18"N	141°2'58"E	12.2	81	72	3510 ± 26	150 ± 2	Silt	Base of steeper ascending slope (semicircular depression)
7	UKEE-140305-3	2014/3/5	37°29'55"N	141°4'57"E	28.1	50	34	105 ± 9	32 ± 7	Silt—medium sand	Gently descending slope
8	UKEE-140226-4	2014/2/26	37°29'60"N	141°4'44"E	26.9	30	N.D.	125 ± 9	35 ± 1	Silt—fine sand	Gently descending slope
9	UKEE-140206-7	2014/2/6	37°30'31"N	141°4'41"E	25.8	30	N.D.	175 ± 4	21 ± 1	Fine sand	Gently descending slope
10	UKEE-140206-8	2014/2/6	37°30'43"N	141°3'10"E	13.8	42	33	22 ± 2	9 ± 1	Fine sand	Gently descending slope
11	UKEE-140227-10	2014/2/27	37°28'34"N	141°4'18"E	19.8	48	15	13 ± 1	8 ± 1	Very fine—fine sand	Gently descending slope
12	UKEE-140304-12	2014/3/4	37°28'11"N	141°2'50"E	10.5	39	35	95 ± 3	27 ± 1	Very fine—fine sand	Flat
13	UKEE-140304-13	2014/3/4	37°28'7"N	141°3'41"E	16.1	26	N.D.	72 ± 2	23 ± 1	Very fine sand	Flat

N.D. not detectable

[a] Just above depth where ^{137}Cs concentrations were below the detection limit (about several Bq kg^{-1} dry) of ^{137}Cs concentration

[b] Wentworth size class
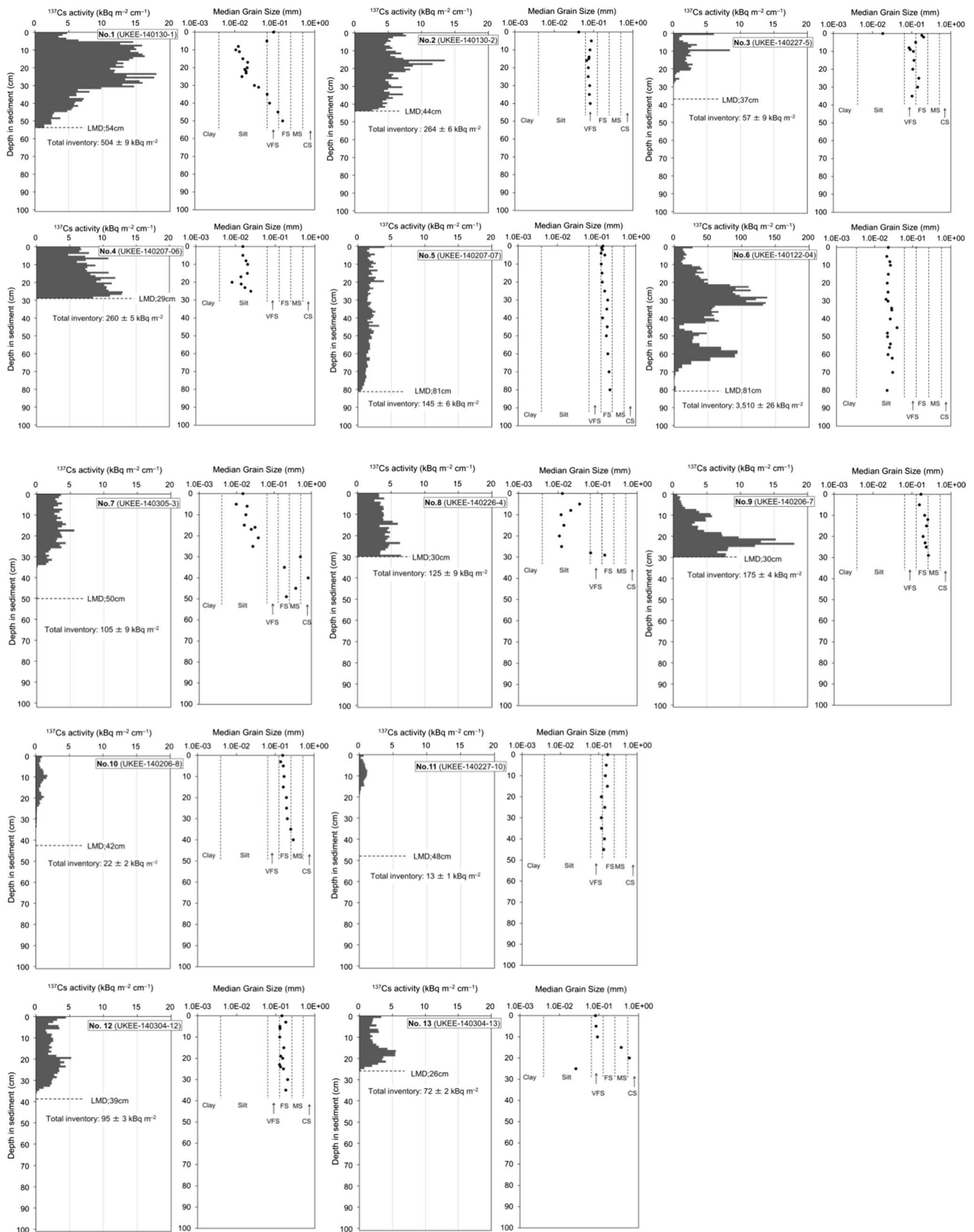
◀**Fig. 5** Vertical distribution of ^{137}Cs activities (kBq m^{-2} cm^{-1}), total inventory per unit (kBq m^{-2}), and median grain size (D50 value) of samples collected via vibrocoring. Size class of D50 value are described according to the Wentworth grain-size scale: clay (<0.004 mm), silt (0.004–0.063 mm), very fine sand (VFS: 0.063–0.125 mm), fine sand (FS: 0.125–0.25 mm), medium sand (MS: 0.25–0.5 mm), and coarse sand (CS: 0.5–1.0 mm). *LMD* lowermost core depth

4 Discussion

Control factors of ^{137}Cs distribution in the seabed sediments in shallow seas will be discussed based on the abovementioned results.

4.1 Influence of seafloor topography

The grain size at sampling location No. 6, which had a remarkably large ^{137}Cs inventory and was in a semicircular depression with steep sides (Figs. 2, 3), corresponds to silt, and the change in grain size is small (Figs. 5, 6). These results suggest that the semicircular depression area is under a low current, which prompts the settling of fine-grained particles, and that the range of this current velocity is nearly constant compared to velocities in the other areas. The current velocity at the bottom layer of each sampling point was observed using an Acoustic Doppler Current Profiler (Workhorse Sentinel: 600 Hz) towed by ships between August and December 2014. The mean shear stress was calculated using the method described by the Japan Society of Civil Engineers (2000). Figure 7 shows the relationship between the mean shear stress and a part of the ^{137}Cs inventories. The cores of the partial ^{137}Cs inventories are the upper 10 cm from the surface of seabed sediments, which were referred to in previous studies, in particular, samples collected in shallow sea with depths less than 100 m (Otosaka and Kato 2014; Black and Buesseler 2014). The averages of the mean shear stresses at sampling location No. 6 were lower (0.1 N m^{-2}) than those at the other sampling locations. These results suggest that the difference in current velocity between the semicircular depression area and the other areas is caused by topographic features. The steep slope around the semicircular depression area appears to play a major role as a topographic barrier in reducing the current velocity. Areas that have similar seafloor topography were not identified in the investigation area, suggesting that distributions with remarkably large ^{137}Cs inventories (more than several thousands of kBq m^{-2}) are strictly limited.

The mean shear stress values at sampling locations Nos. 1 and 4, where the ^{137}Cs inventories were relatively large, are low (Fig. 7). Therefore, the topographic feature corresponding to the "bases of vertical terrain features," as described by Thornton et al. (2013), the base of steeper ascending slopes, can potentially accumulate ^{137}Cs. By contrast, the relationship between mean shear stress and sampling locations is unclear in the low-^{137}Cs-inventory locations (Fig. 7). Especially, at these locations, there are low ^{137}Cs inventory locations (Nos. 10 and 12), despite low mean shear stress values. Further studies, including evaluations of the ^{137}Cs movement processes (e.g., resuspension and transport of ^{137}Cs-bound seabed sediments (Otosaka et al. 2014; Buesseler et al. 2015) and desorption of ^{137}Cs from seabed sediments), are needed.

4.2 Influence of discharge from river basin

The vertical profile of ^{137}Cs distribution in seabed sediments generally showed gradual changes (Ambe et al. 2014; Otosaka and Kato 2014; Black and Buesseler 2014). Vertical profiles similar to those of the ^{137}Cs distribution were observed in this study. By contrast, rapid changes and multiple peaks in the ^{137}Cs distribution were observed at several locations (Nos. 1, 6, and 9). It is likely that these rapid changes and multiple peaks are related to the release of ^{137}Cs from the Ukedo River. Several heavy-rain events, which were considered to be a cause of significant export flux of ^{137}Cs from inland to the coastal region (Nagao et al. 2013), were observed in the Ukedo River Basin from September 2011 to October 2013 (e.g., Typhoon Roke, September 2011; Typhoon Man-yi, September 2013). Rapid changes and multiple peaks of the ^{137}Cs distribution obtained in this study were inferred to be related to pulse-input by the heavy-rain events. In particular, it is likely that the changes in the ^{137}Cs distribution at location No. 6 were strongly affected by differences in the magnitude of ^{137}Cs release with each heavy-rain event because location No. 6 is under a low current, which prompts the settling of fine-grained particles, as mentioned above. However, in this study, there was no evidence to distinguish between rain event inputs related to the release of ^{137}Cs. Therefore, further studies, including an analysis of environmental isotopes (e.g., δ^{13}C and δ^{15}N), are necessary. Other possible mechanisms of ^{137}Cs movement processes, resuspension, and lateral transport of ^{137}Cs-bound seabed sediments (Otosaka et al. 2014; Buesseler et al. 2015) are needed, as well.

4.3 ^{137}Cs inventory in shallow sea

The relationships between ^{137}Cs inventory and water depth obtained in this study, those obtained by Otosaka and Kato (2014), and by Black and Buesseler (2014) are summarized in Fig. 8. For the sake of comparison with results from previous studies, the totals of the upper 10 cm of the ^{137}Cs inventories in this study are also plotted in Fig. 8. As mentioned above, the distribution of the remarkably large ^{137}Cs inventory at sampling location No. 6 was thought to be limited to a specific area; data for this location have
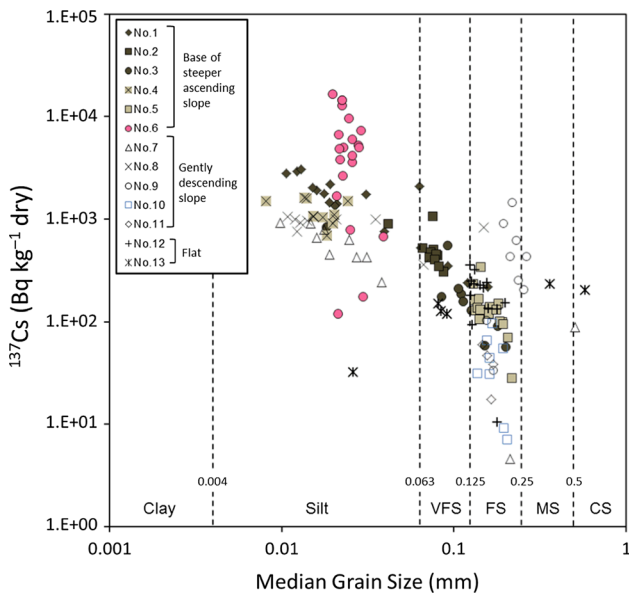
**Fig. 6** Relationship between ^{137}Cs concentration (Bq kg^{-1} dry) and median grain size

been excluded from Fig. 8. The ^{137}Cs inventories of all cores obtained in this study were remarkably larger than those reported by Otosaka and Kato (2014) and Black and Buesseler (2014). These results could be attributed to the longer core length used in this study. Moreover, the ^{137}Cs inventories of the upper 10 cm of the cores were larger than those reported in previous studies, suggesting that the massive ^{137}Cs accumulation in the investigation area can be attributed to the selection of sampling locations near the mouth of the Ukedo River, which is located approximately 5–10 km from the FDNPP. Because many data reported in

previous studies, as shown in Fig. 8, were obtained more than 20 km from the FDNPP and deeper than 30 m, the data of this study have relatively higher values than those of previous studies. In particular, the upper part of the Ukedo River Basin is highly contaminated radiologically, and the annual ^{137}Cs discharge from the Ukedo River into the Pacific Ocean is the highest compared to other rivers in the region. Therefore, the results of this study suggest that the ^{137}Cs distributions near the river mouth, where the basin has high levels of radiological contamination, are considerably affected by the ^{137}Cs discharge from the river basin.

Table 2 presents the predicted ^{137}Cs inventories versus water depth in regions shallower than 100 m calculated using the best-fit exponential regressions obtained in this study and those reported by Otosaka and Kato (2014). The ^{137}Cs inventory at sampling location No. 6 was excluded from the input data of the best-fit exponential regressions given in Table 2. Despite it being difficult to make a strict comparison between the ^{137}Cs inventories based on the abovementioned studies owing to the low correlation coefficients obtained in this study, the predicted ^{137}Cs inventories of all cores in this study were several times larger than those reported by Otosaka and Kato (2014). This result indicates that the earlier ^{137}Cs inventories per unit in seabed sediments from shallow seas, especially, near the river mouth, which has basins with high levels of radiological contamination, were underestimated. However, the surface ratio of seabed sediments based on the abovementioned studies is less than half of the total investigation area. Therefore, the extent of ^{137}Cs distributions along the vertical depth and the surface ratio of seabed sediments should be considered to estimate the ^{137}Cs inventory in shallow seas.

Fig. 7 Relationship between mean shear stress ($n = 8$) and ^{137}Cs inventories. There was a total of 10 cm of ^{137}Cs inventory (kBq m^{-1}) in each core. The *broken lines* show the range between the maximum and the minimum values of shear stress
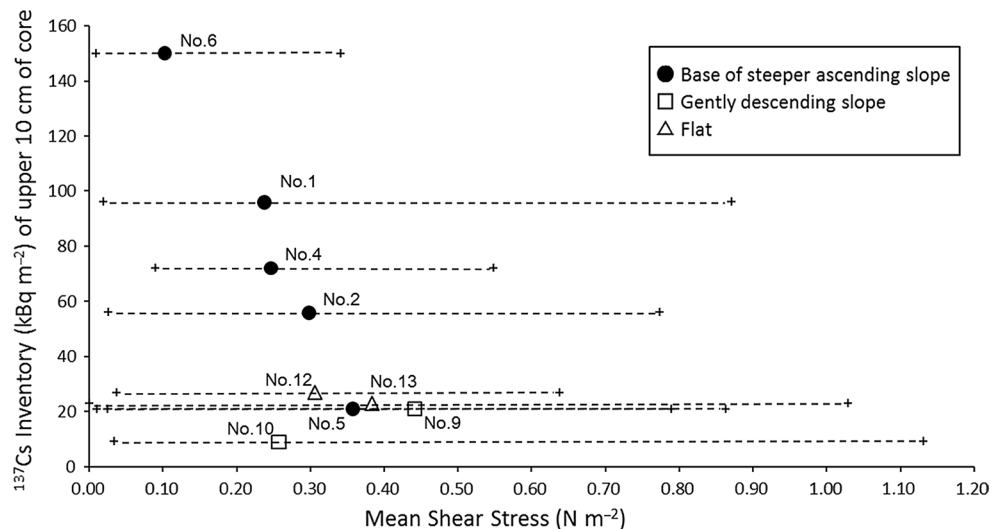
Fig. 8 Relationship between ^{137}Cs inventory and water depth
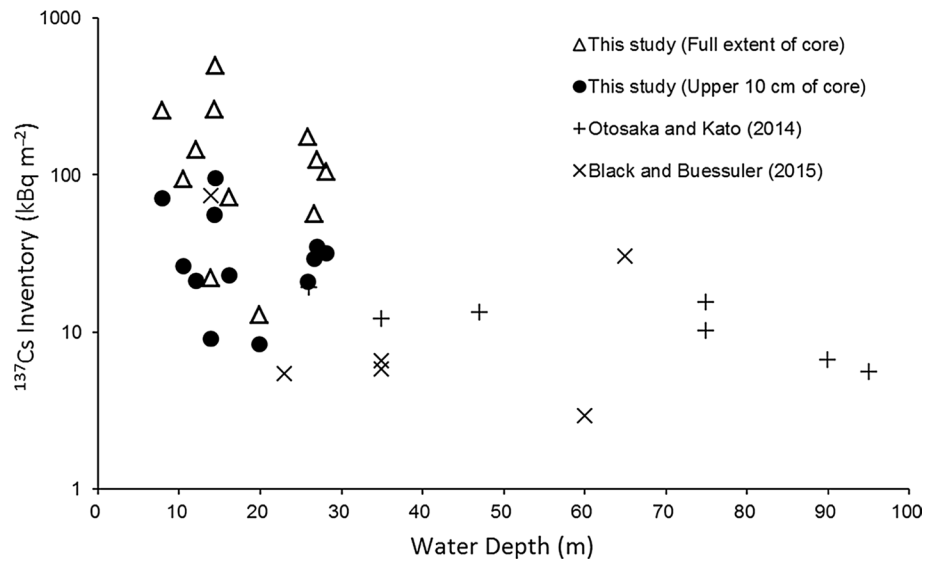
Table 2 Predicted ^{137}Cs inventories versus water depths shallower than 100 m calculated by best-fit exponential regressions

Water depth (m)	This study (full extent of core)	This study (upper 10 cm of core) (kBq m^{-2})	Otosaka and Kato (Otosaka and Kato 2014)
5	146	36	23
10	127	33	22
20	96	27	19
30	73	23	17
50	42	16	13
70	24	11	10
100	10	6	7
Best-fit exponential regression for the ^{137}Cs inventry (kBq m^{-2})	$I = 168.42 \times e^{-0028Z}$ ($r^2 = 0.037$)	$I = 39.033 \times e^{-0.018Z}$ ($r^2 = 0.031$)	$I = 25.011 \times e^{-0.013Z}$ ($r^2 = 0.649$)[a]

Z water depth

[a] Best-fit exponential regression is calculated by the inventories data from stations S2–S8 (Table 1 in Otosaka and Kato 2014)

5 Conclusions

The horizontal and vertical distributions of ^{137}Cs in the seabed sediments in shallow seas of < 30 m depth near the FDNPP were reported. The ^{137}Cs distributions in the seabed sediments were not uniform; however, the ^{137}Cs inventories tended to be concentrated more at the base of steeper ascending slopes around terrace-like seafloors than on the terrace-like seafloors themselves. Based on the relationship between the ^{137}Cs inventory and the mean shear stress, features of the seafloor topography were determined as significant factors controlling the horizontal and vertical distribution of ^{137}Cs in the seabed sediments. Continuous ^{137}Cs distribution at depths greater than 81 cm was observed, indicating that it is difficult to capture the full extent of ^{137}Cs distribution along various vertical depths. Therefore, estimation of the ^{137}Cs inventory in shallow seas should be performed carefully considering the extent of ^{137}Cs distributions along the vertical depth and the surface ratio of the seabed sediments. Moreover, further studies in the area south of the FDNPP are needed to estimate the ^{137}Cs inventory in shallow seas because ^{137}Cs concentration generally tends to be higher in the area south of the FDNPP than in the area north of it (e.g., Kusakabe et al. 2013; Ambe et al. 2014).

fieldwork and measurements. Finally, the authors are grateful to the two anonymous reviewers for their rigorous but positive comments.

References

Ambe D, Kaeriyama H, Shigenobu Y, Fujimoto K, Ono T, Sawada H, Saito H, Miki S, Setou T, Morita T, Watanabe T (2014) Five-minute resolved spatial distribution of radiocesium in sea sediment derived from the Fukushima Dai-ichi Nuclear Power Plant. J Environ Radioact 138:264–275

Black EE, Buesseler KO (2014) Spatial variability and the fate of cesium in coastal sediments near Fukushima, Japan. Biogeosciences 11:5123–5137

Buesseler KO, German RC, Honda MC, Otosaka S, Black EE, Kawakami H, Manganini SJ, Pike SM (2015) Tracking the fate of particle associated Fukushima Daiichi cesium in the ocean off Japan. Environ Sci Technol 49:9807–9816

Dohi T, Ohmura Y, Kashiwadani H, Fujiwara K, Sakamoto Y, Iijima K (2015) Radiocaesium activity concentrations in parmelioid lichens within a 60 km radius of the Fukushima Dai-ichi Nuclear Power Plant. J Environ Radioact 146:125–133

Funaki H, Hagiwara H, Tsuruta T (2014) The behavior of radiocaesium deposited in an upland reservoir after the Fukushima Nuclear Power Plant accident. Mater Res Soc Symp Proc 1665:165–170

Japan Society of Civil Engineer (2000) Manual of hydraulic engineering (in Japanese). Japan Society of Civil Engineers, Japan

JIS (Japan Industrial Standards) (2009) Test method for particle size distribution of soils (JIS A 1204) (in Japanese). http://kikakurui.com/a1/A1204-2009-01.html. Accessed 14 Dec 2016

Kitamura A, Yamaguchi M, Kurikami H, Yui M, Onishi Y (2014) Predicting sediment and cesium-137 discharge from catchments in eastern Fukushima. Anthropocene 5:22–31

Kitamura A, Machida M, Itakura M, Yamada S (2015) Longshore transport modeling of the contaminated sediments in the Fukushima area. 2015AGUFM.B13A0596K

Kubo K, Yanagisawa Y, Yoshioka T, Takahashi Y (1994) Geology of the Namie and Iwaki-Tomioka district (in Japanese with English Abstract). Geol Sur Japan. Niigata (7) No. 46 and 47

Kurikami H, Kitamura A, Yokuda S, Onishi Y (2014) Sediment and ^{137}Cs behaviors in the Ogaki dam reservoir during a heavy rainfall event. J Environ Radioact 137:10–17

Kusakabe M, Oikawa S, Takata H, Misonoo J (2013) Spatiotemporal distributions of Fukushima-derived radionuclides in nearby marine surface sediments. Biogeosciences 10:5019–5030

Mii H (1962) Coastal geology of Tanabe Bay. Tohoku Univ Sci Rep (Geol) 34:1–93

Misumi K, Tsumune D, Tsubono T, Tateda Y, Aoyama M, Kobayashi T, Hirose K (2014) Factors controlling the spatiotemporal variation of ^{137}Cs in seabed sediment off the Fukushima coast: implications from numerical simulations. J Environ Radioact 136:218–228

Mogi A, Iwabuchi Y (1961) Submarine topography and sediments on the continental shelves along the coasts of Joban and Kashi-manada (in Japanese with English Abstract). Geogr Rev Japan 34:159–178

Nagao S, Kanamori M, Ochiai S, Tomihara S, Fukushi K, Yamamoto M (2013) Export of ^{134}Cs and ^{137}Cs in the Fukushima river system at heavy rains by Typhoon Roke in September 2011. Biogeosciences 10:6215–6223

Niizato T, Abe H, Mitachi K, Sasaki Y, Ishii Y, Watanabe T (2016) Input and output budgets of radiocesium concerning the forest floor in the mountain forest of Fukushima released from the TEPCO's Fukushima Dai-ichi Nuclear Power Plant accident. J Environ Radioact 161:11–21

NRA (Nuclear Regulation Authority), Japan (2016) Research on continuous sea area monitoring for radioactive cesium (in Japanese). http://radioactivity.nsr.go.jp/ja/contents/13000/12079/view.html. Accessed 14 Dec 2016

Ono T, Ambe D, Kaeriyama H, Shigenobu Y, Fujimoto K, Sogame K, Nishimura N, Fujikawa T, Morita T, Watanabe T (2015) Concentration of ^{134}Cs + ^{137}Cs bonded to the organic fraction of sediments offshore Fukushima, Japan. Geochem J 49:219–227

Otosaka S, Kato Y (2014) Radiocesium derived from the Fukushima Daiichi Nuclear Power Plant accident in seabed sediments: initial deposition and inventories. Environ Sci Process 16:978–990

Otosaka S, Kobayashi T (2012) Sedimentation and remobilization of radioecsium in the coastal area of Ibaraki, 70 km south of the Fukushima Dai-ichi Nuclear Power Plant. Environ Monit Assess 185:5419–5433

Otosaka S, Nakanishi T, Suzuki T, Satoh Y, Narita H (2014) Vertical and lateral transport of particulate radiocesium off Fukushima. Environ Sci Technol 48:12595–12602

TEPCO (Tokyo Electric Power Co.) (2016) TEPCO news press release. http://www.tepco.co.jp/decommision/monitoring/index-j.html. Accessed 14 Dec 2016

Thornton B, Ohnishi S, Ura T, Odano N, Sasaki S, Fujita T, Watanabe T, Nakata K, Ono T, Ambe D (2013) Distribution of local ^{137}Cs anomalies on the seafloor near the Fukushima Dai-ichi Nuclear Power Plant. Mar Poll Bull 74:344–350

Yamada S, Kitamura A, Kurikami H, Yamaguchi H, Malins A, Machida A (2015) Sediment transport and accumulation in the Ogaki dam in eastern Fukushima. Environ Res Lett 10:014013. doi:10.1088/1748-9326/10/1/004013

Yamaguchi M, Kitamura A, Oda Y, Onishi Y (2014) Predicting the long-term ^{137}Cs distribution in Fukushima after the Fukushima Dai-ichi Nuclear Power Plant accident: a parameter sensitivity analysis. J Environ Radioact 135:135–146

Yoshimura K, Onda Y, Sakaguchi A, Yamamoto M, Matsuura Y (2015) An extensive study of the concentrations of particulate/dissolved radiocaesium derived from the Fukushima Dai-ichi Nuclear Power Plant accident in various river systems and their relationship with catchment inventory. J Environ Radioact 139:370–378